AD-A093 064 CORNELL UNIV ITHACA NY DEPT OF CHEMISTRY F/G 7/4
A STUDY OF SECONDARY MOLECULAR ION FORMATION IN RARE EARTHS AND--ETC(U)
DEC 80 D T HODUL, W C HARRIS, G H MORRISON N00014-80-C-0538
UNCLASSIFIED TR-4 NL

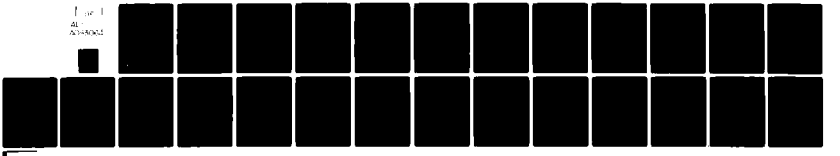

END
DATE FILMED
1-81
DTIC

OFFICE OF NAVAL RESEARCH

Contract N00014-80-C-0538

Task No. NR 051-736

Technical Report No. 4

A Study of Secondary Molecular Ion Formation in Rare Earths and Rare Earth Oxides

D. T. Hodul, W. C. Harris and G. H. Morrison

Prepared for Publication

in

Radiation Effects

Cornell University

Department of Chemistry

Ithaca, N. Y. 14853

December 15, 1980

SECURITY CLASSIFICATION OF THIS PAGE (When Data Entered)

REPORT DOCUMENTATION PAGE

READ INSTRUCTIONS BEFORE COMPLETING FORM

1. REPORT NUMBER: Technical Report No. 4	2. GOVT ACCESSION NO.: AD-A093 064
3. RECIPIENT'S CATALOG NUMBER:	
4. TITLE (and Subtitle): A Study of Secondary Molecular Ion Formation in Rare Earths and Rare Earth Oxides.	5. TYPE OF REPORT & PERIOD COVERED: Interim Technical Report.
	6. PERFORMING ORG. REPORT NUMBER:
7. AUTHOR(s): D. T. Hodul, W. C. Harris and G.H. Morrison	8. CONTRACT OR GRANT NUMBER(s): N00014-80-C-0538
9. PERFORMING ORGANIZATION NAME AND ADDRESS: Department of Chemistry, Cornell University, Ithaca, New York 14853	10. PROGRAM ELEMENT, PROJECT, TASK AREA & WORK UNIT NUMBERS: NR 051-736
11. CONTROLLING OFFICE NAME AND ADDRESS: ONR (472), 800 N. Quincy St., Arlington, Va. 22217	12. REPORT DATE: December 15, 1980
	13. NUMBER OF PAGES: 24 pp.
14. MONITORING AGENCY NAME & ADDRESS(if different from Controlling Office)	15. SECURITY CLASS. (of this report): Unclassified
	15a. DECLASSIFICATION/DOWNGRADING SCHEDULE

16. DISTRIBUTION STATEMENT (of this Report)

Approved for public release; distribution unlimited

17. DISTRIBUTION STATEMENT (of the abstract entered in Block 20, if different from Report)

18. SUPPLEMENTARY NOTES

Prepared for publication in Radiation Effects

19. KEY WORDS (Continue on reverse side if necessary and identify by block number)

Ion microscope, secondary ion mass spectrometry, digital image processing, ion implantation.

20. ABSTRACT (Continue on reverse side if necessary and identify by block number)

Secondary atomic and molecular ion energy spectra have been obtained for several rare earth and rare earth oxide samples. The energy dependencies of the diatomic ions were found to be a product of the energy dependencies of the atomic ions. Qualitative agreement of this product rule is also found for larger clusters. A recombination mechanism for molecular formation is demonstrated to be consistent with these results. Several preliminary ion implant studies are presented to give further insight into the recombination model.

DD FORM 1 JAN 73 1473

SECURITY CLASSIFICATION OF THIS PAGE (When Data Entered)

A STUDY OF SECONDARY MOLECULAR ION FORMATION IN RARE EARTH AND RARE EARTH OXIDES

D. T. Hodul, W. C. Harris and G. H. Morrison

Department of Chemistry
Cornell University
Ithaca, N.Y. 14853

ABSTRACT

Secondary atomic and molecular ion energy spectra have been obtained for several rare earth and rare earth oxide samples. The energy dependencies of the diatomic ions were found to be a product of the energy dependencies of the atomic ions. Qualitative agreement of this product rule is also found for larger clusters. A recombination mechanism for molecular formation is demonstrated to be consistent with these results. Several preliminary ion implant studies are presented to give further insight into the recombination model.

1. INTRODUCTION

Secondary molecular ion production has been observed for a wide variety of materials and a large range of experimental conditions.[1-11] The complexity of the sputtering process is reflected in the diversity of theoretical approaches that have been generated for both atomic[12-20] and cluster ion[21-27] formation processes. The dependence of secondary emission angle and energy on experimental parameters, for example primary ion mass, angle, energy, or sample orientation, has been used to test the predictions and these models.[22,25,28-33] In addition, sputtering models must be capable of explaining the effects that reactive primary ions and adsorbed gases have on ionization yields.[34-36] Computer simulations have demonstrated the plausibility of both the collision cascade construct and the recombination mechanism of molecular ion formation.[24,37-40] Also an exponential dependence of ion yield on ionization potential has been consistently demonstrated.[13] While a clear picture of sputtering has not emerged, these established features are essential preconditions for any model.[41,42]

In addition to the insights about the nature of the sputtering process outlined above, the study of secondary molecular ions hopes to provide answers applicable in surface analysis, molecular chemistry, and surface structure and bonding. Energy discrimination against molecular species has been used to improve the detection limits of SIMS analysis[43,44] and the use of moleculars for impurity analysis has been demonstrated.[45,46] A review of studies of cluster ions for surface structural analysis is given by Blaise.[47] Garrison et al.[40] have proposed experiments for similar application by measuring secondary ion angle distributions. Further, ion bombardment of surfaces provides a method for producing unusual small ion species for cyclotron

resonance, laser, and reaction studies. Some bonding ideas dealing with such species already have been put forth.[5,48-51]

In this paper we report results of several experiments performed to understand the mechanism for metal oxide molecular ion formation on rare earth and rare earth oxide surfaces during ion bombardment. A preliminary study of copper implanted with indium and gallium was done to assess the validity of models for molecular ion formation, i.e. to determine whether the $GaIn^+$ signal was proportional to the product of the In^+ and Ga^+ signals. The effects of an oxygen primary beam are discussed in this context. The results of several other implant studies are also given.

Energy spectra of positive and negative molecular oxide and atomic ions were obtained for a rare earth metal, Gd foil and for pressed pellets of the oxides Dy_2O_3, Gd_2O_3 and Tm_2O_3. An oxygen primary beam was used for all the samples and the results were compared to an argon beam analysis of Gd_2O_3. Mechanisms for cluster ion formation are presented and the results are shown to be consistent with a recombination model. Finally, we indicate the broader implications of these interpretations and outline further studies.

2. EXPERIMENTAL

Ion implantation is a useful tool in SIMS studies. When ion implanted samples are depth profiled, the implanted species has an easily recognized gaussian shape. This is particularly useful when working with molecular secondary ions, for the shape of the molecular profile will reflect the concentration behavior of its constituent parts.[45,46,52,53] A high purity polished copper sample was implanted with 250 keV Ga^+ and In^+ at fluences of 10^{15} atoms/cm^2 using an AI 300R implanter. Two polished [100] silicon samples were implanted, one with

250-keV Si^+ at a fluence of 1.3×10^{15} and the other with Al^+ at a fluence of 10^{13} atoms/cm^2 and GaAs single crystal with 250-keV Cs^+ at a fluence of $2 \times 10^{14}/cm^2$. The sources of implantation were gallium and indium metal, SiF_4, $AlCl_3$ and CsI. Solids were run using the oven source.

The rare earth sample was a high purity foil from Alfa Ventron: Gd(M3N). No polishing preparation was necessary for the pure metal. The oxide samples were powdered Dy_2O_3 (Alfa 99.9), Gd_2O_3 (Alfa 99.9%), and Tm_2O_3 (Alfa 99.999%). The powders were mixed with 95% silver powder (Cominco American 59 Grade), and pressed into pellets. The silver was needed to prevent charging of the sample by the primary beam during analysis. The pressing process provided smooth sample surfaces. Rare earth and rare earth oxides were chosen for this study since their high mass reduces mass interferences from vacuum contaminants and impurities.

SIMS analysis was performed on a CAMECA IMS-300.[54] The Ga and In double implant, aluminum in silicon, and cesium in gallium arsenide profiles were obtained using a positive oxygen primary beam ($O_2^+/O^+ \simeq 10$) of 1 μA rastered over 400 μm x 400 μm area. Si^+, Si_2^+ and Si_3^+ analysis of silicon in silicon used a 180 nA primary beam rastered over a similar area. Silicon in silicon for silicon oxides used a 20 nA primary, negative ion detection. The rare earth sample was analyzed using an unrastered 1 μA positive primary beam for both oxygen and argon studies. In the positive primary/positive secondary mode the primary angle of incidence is ~38°, the energy is 5.5 keV. The positive/negative mode parameters are ~57° and 14.5 keV, respectively. Secondaries are detected normal to the surface. The vacuum was 10^{-7} torr. The ESA was tuned to maximum signal for a 4.5-keV sample voltage and an aperture used when necessary to reduce detector (ion counting electron multiplier) saturation. Energy spectra were obtained by lowering the sample voltage resulting

in the selection of higher energy secondaries.[55] The primary beam was refocussed after each voltage change. Since a deconvolution of the energy spectra[56] was not performed, a band pass of < 15 eV can be assumed. The spectra obtained are listed in Table I.

3. MOLECULAR SPUTTERING

While many aspects of sputtering still remain unresolved, the collision cascade has been accepted as essential to any description of this process and must be a part of models of secondary molecule formation. The time and spatial scales of the collision cascade will depend mainly on the primary ion energy but also for example, on incident angle and sample chemistry. For the 5.5 and 14.5 keV primary energies used for these experiments a cascade of linear dimensions of $\sim$100 Å is appropriate. For secondary atom emission the time of the cascade can be broken into three regimes: 1) instant momentum transfer ($\sim 10^{-14}$ sec), 2) many collision momentum transfer ($\sim 10^{-12} - 10^{-13}$ sec), and 3) thermal process (roughly $\gg 10^{-10}$ sec). All of these regimes may produce secondary molecules through aggregate ejection, but recombination to form clusters will not occur in thermal processes as coordination of 10^{-13} sec is needed to form bonds. Similarly, atomic recombination above the surface to form molecules will occur only from a single cascade; here again for spatial coordination reasons. If the sample is homogeneous on the order of cascade dimensions or if only neighbors less than several atoms distant can recombine into molecules, no boundary effects need be considered. In samples with heterogeneous regions the order of the cascade, the effects of the cascade size can be important.

Studies of secondary ion energy and angle dependencies can reveal fundamental aspects of the sputtering process. Cascade models of secondary emission predict a low energy maximum in atomic signal levels of a few electron volts and a high energy tail with an energy dependence of $E^{-1/2}$. When secondary ion energy spectra are measured, the energy dependence of ionization must also be considered when analyzing the results. The energy dependence of ionization depends on a large number of factors, primary ion parameters, matrix composition and crystal orientation, detection angle and vacuum conditions. In general, the secondary ion energies will be a product of the cascade dependence and the ionization dependence. However, when an oxygen primary beam is used, the resulting secondary ion dependence appears to originate solely from cascade considerations.[32] Similar results are obtained for oxide matrices and for oxygen adsorption on the sample surface. This has been interpreted as virtual energy independence of the ionization mechanism caused by the presence of oxygen.[36,55,57] This behavior was exploited to simplify the study of molecular ion formation.

Models of molecular secondary ion formation during sputtering are of two main types, aggregate ejection and recombination. Clusters formed through aggregate ejection are sputtered from the surface as a single entity. Consequently, such molecules consist only of atoms which were adjacent on the surface. Rearrangement and fragmentation after sputtering is possible. Ionization processes for aggregate ejection mechanisms can occur during sputtering or after ejection. The former mechanism is reasonable for both positive and negative species, while post-sputtering ionization for positive clusters can proceed through ejection of an electron from a vibronically excited secondary. Negative ions must form from electron capture of a surface electron; in this

case the electron affinity of the molecular species and the bond energy of the molecule are important considerations in developing models of molecular formation. Recent results on a series of ion implanted semiconductors indicates that for the systems studied post aggregate ejection ionization is unlikely in forming negative secondaries.[46]

Recombination mechanisms for cluster formation seem improbable at first glance. However, computer simulations of the sputtering process demonstrate that recombination of atomic species above the surface is likely, if the relative energy of the recombining atoms is less than the bond energy of the molecule.[24,37-40] Analogous to aggregate ejection, one can envision several ionization schemes for post recombination ionization. Since the recombining atoms will exhibit a range of relative energies up to the bond energy or even slightly greater for electronically excited bound states, many excited molecular neutrals may relax to molecular cations by ejection of an electron. Anions may form through recombination with a secondary electron or capture of an electron from the surface. We expect such anionization processes to be improbable as the computer simulations predict recombination to be several atomic spacings above the surface, too far from the molecule to polarize the surface and capture the needed electron. Further, we argue reaction with a secondary electron must be coordinated as to be practically indistinguishable from prerecombination ionization mechanisms.

Precombination ionization can be viewed as the recombination of a secondary ion with neutral secondary species. In such a case, the ionization yield of a molecular ion is dependent on the ionization yields of its constituents, and as always the bond energy of the cluster.

Two observables can be measured for both molecules and constituent atoms to elucidate the formation processes, 1) the concentration dependence of ion yields at a specified energy, and 2) the energy dependence of ion yields. For homogeneous surfaces the number of secondary molecular ions is expected to depend on the product of the atomic concentrations of the species contained in the molecular secondary.[47] When static (primary current < 1 nA/cm^2) conditions are used and if molecules form through an aggregate mechanism, structural information about the surface can be obtained (see reference 47 sec V-3, III-4). However, under dynamic conditions (primary current $\simeq 25$ μA/cm^2) used for this study the surface is randomized sufficiently to render aggregate and recombination indistinguishable by a study of concentration dependence, and we have used the energy dependence of the secondary species for this purpose.

The following is a representative list of plausible recombination reactions; a formalism similar to kinetic theories of gaseous reactions is used.

$$A^{\pm} + B \longrightarrow AB^{\pm} \qquad (3.1)$$

$$A + B \longrightarrow AB^{*} \longrightarrow AB^{+} + e^{-} \qquad (3.2)$$

$$A + B \longrightarrow AB \qquad (3.2a)$$

$$AB + e^{-} \rightarrow AB^{-} \qquad (3.3b)$$

$$AB^{\pm} + B \longrightarrow ABC^{\pm} \qquad (3.4)$$

For the AB^+ dimer an expression can be written:

$$[AB^+] = k_1 [A^+][B] + k_2 [A][B^+] + k_3 [A][B] \qquad (3.5)$$

where [ ] indicates the ion yield per cascade for the species in the brackets, and k_1, k_2 and k_3 reflect the probability of their respective reactions' contribution to the recombination molecule. Similarly, the energy spectrum of

molecule will be the sum of the products of the energy spectra of the atomic species for each reaction:

$$[AB^+(E)] = k_1\,[A^+(E)][B(E)] + k_2\,[A(E)][B^+(E)] + k_1\,[A(E)][B(E)] \qquad (3.6)$$

where for example $A^+(E)$ is the ion yield of A^+ as a function of energy. Since an oxygen primary was used for this study, the high energy dependencies of the atomic spectra are expected to exhibit cascade-like character, i.e. $< E^{-1/2}$, implying both neutral and ion atomic secondaries will have the same functional form. The energy dependence of $AB^{\pm}$ is therefore expected to be proportional to the product of the energy dependencies of $A^{\pm}$ and $B^{\pm}$. Larger clusters will have energy spectra which are more complicated, but some qualitative conclusions on these ions may be possible. For example, trimers which have approximately a dimer-like energy dependence suggest a molecular formation mechanism where a sputtered aggregate dimer recombines with a monomer, since we assume aggregate ejection will have approximately atomic-like energy dependencies. The energy independence of ionization processes for oxides and oxygen primary beams again is used to justify this assumption. The energy dependence of a pure recombination, i.e. three center, trimer is expected to have an energy dependence which is the product of the three atomic dependencies of the constituent species.

Strictly, both neutral and ion spectra should be measured, and the products of such spectra used to determine the molecular spectra. If, for example, (3.6) was used as a model $AB^{\pm}$ energy dependence, k_1, k_2 and k_3 could be calculated by measuring $AB^{\pm}(E)$, $A(E)$, $B(E)$, $A^{\pm}(E)$ and $B^{\pm}(E)$, resulting in an extremely detailed picture of the $AB^{\pm}$ molecular formation process. To more generally describe the process several additional factors can be included in such a product energy spectra analysis. 1) The effects of bond energy and

excited product states can be convoluted into the product scheme. At energies close to the bond energy, this consideration will be significant but will not greatly effect analysis in the high energy tail region. 2) The secondary angular distribution can also be important, but as bond energies are small, it will have little affect on the distinction of mechanisms.

4. RESULTS

Several ion implant studies were performed to evaluate the general validity of both the aggregate and recombination mechanisms by determining if molecule formation showed the expected concentration dependence. Ion implants are valuable in providing a known gaussian depth profile with a wide concentration range. ← Figures 1+2

Figure 1 shows a depth profile of the Cs implant (GaAs sample). The Cs^+ and Cs_2^+ signals were monitored and the Cs_2^+ signal was found to vary as the square of the Cs^+ when the signal peaks are normalized. The extremely low Cs_2^+ signal likely reflects a weak Cs-Cs bond.

The results of the Ga and In implants in polished copper are given in Figure 2. The Ga^+, In^+ and $GaIn^+$ signals were monitored. The $GaIn^+$ signals behave as expected, and can be seen to be the product of the Ga^+ and In^+ signal when all the signals are normalized. The high $GaIn^+$ signal is indicative of a strong Ga-In bond. A small mass interference at m/e = 184 is responsible for the slight discrepency of concentration product behavior for data in the gaussian tail. ← Figures 3, 4+5

While the above results agree with expectation, a degree of caution in molecular studies is warranted, and exemplified by the following implant profile studies. Figure 3 shows a depth profile of Al^+ and Al_2^+ for the aluminum implanted

sample and is indicative of anomalies encountered in SIMS analysis of implanted silicon materials. Something quite different from the squared gaussian Al_2^+ signal is observed. Precipitate formation or unusual implant damage are both plausible explanations of this behavior. More remarkable are the results of the silicon implant in silicon. For this system chemical matrix effects will be absent. SIMS signals for SiO^+, SiO_2^+, Si_2^+ and Si_3^+ were monitored and the resulting depth profiles shown in Figures 4 and 5. For the 1-μA primary a slight increase in all the Si signals is observed near the expected implant maxima, and anomalous prepeaks seen for Si_2^+. Similar anomalies are seen for Si_2^+ and Si_3^+ in the 180-nA analysis. These molecular prepeaks have been observed in our laboratory in other implanted silicon materials. While crystal damage during implantation is the likely cause of this unusual behavior, further studies[58] are needed to verify such reasoning.

A few comments on instrumental discrimination are needed before the results of energy spectra studies are presented. Of primary importance are the effects of the secondary ion acceleration voltage and the immersion lens, on the energy band pass of the system. Methods have been devised[56] and used[32,33] to correct the non-linear energy response of the immersion lense. However, the narrow slit widths ($\sim$1 eV before the ESA) used in these methods result in signals which are close to the system noise in the high energy offset region of interest in this study. For this reason we have used a large slit width and rely on the natural response of the immersion lens[55,59] to fix the band pass. Roughly, the response is linear for 0-10 eV and rapidly falls to about 10% of this value at 15 eV; therefore a 15 eV band pass is quoted.

As a consequence of the methods used to produce detectable signals at high energies, the detector was occasionally saturated (> 10^6 cps) at low energies. In such cases an aperture yielding 0.02 times[52] the no aperture response was used and compared to the results where no aperture was used. This procedure produced no significant effect on conclusions of molecular formation mechanisms. For reproducibility the primary beam and vacuum were kept to 5% and 10% deviation during a single sample run.

Results of the rare earth studies are shown in Figures 6 through 10, and are plotted as log of signal versus secondary ion energy. While for a cascade model signal versus log energy plot is most appropriate for determination of the exponential dependence of the energy, we have chosen a representation which more clearly presents the data yet still allows for easily interpreting energy product behaviors for recombined molecules. Generally, monatomic ions had a spectrum with a slope of 0.01 $\frac{\log (cps)}{eV}$ and, consistent with a recombination process, diatomics had twice this value and triatomic almost three times this slope. Specifics and anomolies are discussed below.

5. DISCUSSION

The results of this study demonstrate that the great majority of secondary molecular ions form from recombination of atomic species above the surface. Several cases where behavior deviates significantly from recombination predictions can be used to suggest a more detailed picture for these specific molecular ions.

← Figure 6

For the Dy_2O_3 pellet the Dy^+ signal falls off more slowly than exponently and therefore at high energy more slowly than the typical monatomic (See Figure 6). The Dy^- signal falls off more rapidly than the typical monatomic energy dependence, while DyO_2^- falls faster than three times the monatomic value. This suggests a three center mechanism where the large Dy^- fall off causes the larger than expected trimer behavior:

$$Dy^- + O + O \rightarrow DyO_2^- \qquad (5.1)$$

However, as the DyO_2^- signal is larger than the Dy^- signal, the following mechanism must also contribute significantly to production of DyO_2^-.

$$Dy + O^- + O \rightarrow DyO_2^- \qquad (5.2)$$

Similarly the DyO_2^+ energy dependence is less than three center and suggests the following competing mechanisms for the positive dioxide ion:

$$Dy^+ + O + O \rightarrow DyO_2^+ \qquad (5.3a)$$

$$Dy^+ + O_2 \rightarrow DyO_2^+ \qquad (5.3b)$$

Since the DyO^+ signal is much less than the Dy^+ signal, no mechanism analogous to (5.2) need be postulated. The dysprosium diatomic species behaved as recombination molecules.

← Figures 7 & 9

Both the diatomic secondary ions and GdO_2^+ showed the same dependencies as their dysprosium counterparts (See Figure 7). For the Gd_2O_3 pellets the O^+ ion was monitored and fell more slowly than atomic dependence. Data for this sample using an argon primary produced a different secondary energy spectrum only in the case of O^+, where an atomic dependence was seen (See Figure 8). This suggests that part of the oxygen primary scattered without reacting with the surface, giving rise to high energy O^+ species undistinguishable from true O^+ secondary ions.

← Figure 12

Again the Tm_2O_3 data for diatomics and TmO_2^+ are the same as the two previous rare earth oxide samples (See Figure 10). As expected, after normalization for relative transmittance of the aperture, the Tm^+ and TmO^+ yields are the same, implying that the choice of large ESA slit width and a large band pass are vaid for interpreting molecular mechanisms.

The O_2^- molecule was monitored in both the Tm_2O_3 pellet and the gadolinium foil. Two explanations for the monatomic energy dependence of a diatomic secondary can be devised. Most plausible is that the O_2^- is ejected as an aggregate and therefore has a simple cascade-like energy dependence. Less likely is a scattering process analogous to the O^+ case discussed above. During scattering, the O_2^+ from the primary beam needs to acquire two electrons from the surface, intuitively less appealing than aggregate ejection of O_2^-. All other molecules formed by the foil samples behaved as recombination species.

While a detailed study of all secondary species is needed to determine the detailed features of secondary molecule chemistry, a pattern consistant with chemical intuition does emerge from the data. High signals are obtained for molecules with the rare earth in the plus three states, eg. DyO^+ and Dy_2^-. The use of such oxidation state intuition and the observed dominance of recombination mechanisms can therefore be used to solve analytical problems of species identification and mass interferences in samples of unknown composition.

The results of this study suggest several future experiments on molecular formation during sputtering.

1) Double implants and dimers of single implants may be used to determine relative bond energies of diatomic species. For example Al,

Ga and In implanted singly and in pairs would be depth profiled for Al_2^+, Ga_2^-, In_2^+, $AlGa^+$, $AlIn^+$ and $GaIn^+$ at several energies. The relative signal levels will reflect relative bond strengths of the diatomic species, and the energy spectra may be used to determine a detailed formation mechanism. In cases where aggregates form, molecular ionization potentials (or electron affinities) could be determined from an LTE-like analyses.[13]

2) Dimer analysis of implants may be used for guides to precipitates or damage formed during implantation.

3) Further oxide versus metal studies with an argon primary can be expected to contribute to a chemical understanding of the metal surface. For example, the comparison of metal cluster ion yields in the oxide and metal can be used to extract information about the ionization process, and hence suggest the state of the surface.

ACKNOWLEDGEMENTS

Acknowledgement is given to D. Leta, C. Lee, and G. Harris for their assistance in implantation preparations, as well as the use of the ion implantation facilities of the National Research and Resource Facility for Submicron Structures at Cornell.

This work was supported by the National Science Foundation, the Office of Naval Research, and the Cornell Materials Science Center.

REFERENCES

1. G. Hortig and M. Muller, Z. Phys., 221, 119 (1969).

2. G. Staudenmaier, Rad. Effects, 13, 87 (1972).

3. R.F.K. Herzog, W.P. Poschenrieder, and F.G. Satkiewicz, Rad. Effects, 18, 199 (1973).

4. A. Shepard, R.W. Hewitt, G.J. Slusser, W.E. Baitinger, R.G. Cooks, N. Winograd, W.N. deGlass, A. Varon, and G. Devant, Chem. Phys. Lett., 44, 371 (1976).

5. M. Leleyter and P. Joyes, J. Phys. (Paris), C2, 11 (1977).

6. M. Riedel, T. Nenadovic, and B. Perovic, Magy. Kem. Polv., 83, 499 (1977).

7. J.A. Taylor and J.W. Rabalais, Surf. Sci., 74, 229 (1978).

8. F.M. Devienne, M. Teisseire, and R. Combarieu, C.R. Hebd. Seances Acad. Sci. Ser., C288, 1 (1979).

9. G. Lancaste, F. Honda, Y. Fukuda, and J. Rabalais, Int. J. Mass Spec. & Ion Phys., 29, 199 (1979).

10. F. Honda, Y. Fukuda, and J.W. Rabalais, J. Chem. Phys. 70, 4834 (1979).

11. N.K. Dzhemilev and R.T. Kurbanov, Izv. Akad. Nauk SSR Ser. Fiz, 43, 606 (1979).

12. P. Sigmund, Phys. Rev., 184, 383 (1969).

13. C.A. Andersen and J.R. Hinthorne, Anal. Chem., 45, 1421 (1973).

14. P. Joyes, Rad. Effects, 19, 235 (1973).

15. J.M. Schroer, T.N. Rhodin, and R.C. Bradley, Surf. Sci., 34, 571 (1973).

16. Z. Svroubek, Surf. Sci., 44, 47 (1974).

17. M. Cini, Surf. Sci., 54, 71 (1976).

18. F. C. Rüdenauer, W. Steiger, and H.W. Werner, Surf. Sci., 54, 553 (1976).

19. H.G. Prival, Surf. Sci., 76, 443 (1978).

20. K.R. Pollitt, J.C. Robb, and D.W. Thomas, Nature, 272, 436 (1978).

21. P. Joyes, J. Phys., B4, L15 (1971).

22. P. Joyes, J. Phys. Chem. Solids, 32, 1269 (1971).

23. K. Wittmaack and G. Staudenmaier, Appl. Phys. Lett., 27, 318 (1975).

24. I.S. Bitenskii and E.S. Parilis, Zh. Tehn. Fiz, 48, 1941 (1978).

25. F. Honda, G.M. Lancaster, Y. Fukuda, and J.W. Rabalais, J. Chem. Phys., 69, 4931 (1978).

26. A.E. Moran and H.W. Werner, J. Chem. Phys., 68, 3900 (1978).

27. K. Wittmaack, Phy. Lett., A69, 322 (1979).

28. E. Dennis and R.J. MacDonald, Rad. Effects, 13, 243 (1972).

29. G. Staudenmaier, Rad. Effects, 18, 181 (1973).

30. G.P. Können, A. Tip, and A.E. deVries, Rad. Effects, 21, 269 (1974).

31. G.P. Können, A. Tip, and A.E. deVries, Rad. Effects, 26, 23 (1975).

32. M.A. Rudat and G.H. Morrison, Int. J. Mass Spec. & Ion Phys., 30, 197 (1979).

33. M.A. Rudat and G.H. Morrison, Surf. Sci., 82, 549 (1979).

34. M. Prager, Appl. Phys., 8, 361 (1975).

35. V.R. Deline, W. Katz, C.A. Evans, and P. Williams, Appl. Phys. Lett., 33, 832 (1978).

36. M.A. Rudat and G.H. Morrison, Int. J. Mass Spec. & Ion Phys., 30, 233 (1979).

37. D.E. Harrison and C.B. Delaplain, J. Appl. Phys., 47, 2252 (1976).

38. N. Winograd, D.E. Harrison, and B.J. Garrison, Surf. Sci., 78, 467 (1978).

39. B.J. Garrison, N. Winograd, and D.E. Harrison, J. Chem. Phys., 69, 1440 (1978).

40. B.J. Garrison, N. Winograd, and D.E. Harrison, J. Vac. Sci. Technol., 16, 789 (1979).

41. G. Blaise and A. Nourtier, Surf. Sci., 90, 495 (1979).

42. P. Williams, Surf. Sci., 90, 588 (1979).

43. N. Shimizu, M.P. Semet, and G.J. Allegre, Geochim. et Cosmochim. Acta, 42, 1321 (1978).

44. G. Slodzian, Surf. Sci., 48, 161 (1975).

45. D.P. Leta and G.H. Morrison, Anal. Chem., 52, 514 (1980).

46. D.T. Hodul, W.C. Harris, and G.H. Morrison, submitted to Int. J. Mass Spec. & Ion Phys.

47. G. Blaise "Materials Characterization Using Ion Beams", Plenum Pub. Corp., New York 1976 eds. J.P. Thomas and A. Cachard, p.143.

48. A.E. Morgan and H.W. Werner, J. Microsc. Spectrosc. Electron, 3, 495 (1978).

49. G.M. Lancaster, F. Honda, Y. Fukuda, and J.W. Rabalais, Chem. Phys. Lett. 59, 356 (1978).

50. M.H. Rodriguez and H.E. Beske, Adv. Mass Spectrom., 7A, 593 (1978).

51. R.J. Day, S.E. Unger, and R.G. Cooks, JACS, 101, 499 (1979).

52. D.P. Leta, Ph.D. Thesis, Cornell University (1980).

53. D.P. Leta and G.H. Morrison, Anal. Chem., 52, 277 (1980).

54. G.H. Morrison and G. Slodzian, Anal. Chem., 47, 932A (1975).

55. M.A. Rudat, Ph.D. Thesis, Cornell University (1979).

56. G. Slodzian, "Secondary Ion Mass Spectrometry", NBS Special Pub. 427, Government Printing Office, Washington, D.C., p. 33 (1975).

57. A. Krauss, private communication.

58. DaChang Zhu and G.H. Morrison to be published.

59. CAMECA Manual IMS-300.

Table I. Energy Spectra Measured

Primary/Secondary	Sample	Species Monitored
$O,^{+}O_2^{+}/+$	Dy_2O_3	Dy^+, DyO^+, DyO_2+
	Gd_2O_3	Gd+, GdO^+, GDO_2^+
	Tm_2O_3	O^+, $O_2^+Tm^+$, TmO^{+*}, TmO_2^+
	Gd	O^+, O_2^+, Gd^+, GdO^+, GdO_2^+
O^+, $O_2^{+}/-$	Dy_2O_3	D_y^-, DyO^-, DyO_2^-
	Gd	O^-, O_2^-, Gd, GdO^-
$Ar^+/+$	Gd_2O_3	O^+, O_2^+, Gd^-, GdO^+, GdO_2^+
$Ar^+/-$	Gd_2O_3	O^-, O_2^-

* Two apertures used because of large signals

CAPTIONS

Figure 1 Depth profile of ^{133}Cs implanted GaAs.

Figure 2 Depth profile of a polished Cu sample implanted with ^{69}Ga and ^{115}In yielding the $GaIn^+$ molecular signal as well as Ga^+ and In^+.

Figure 3 Depth profile of $^{27}Al^+$ implanted Si showing anomalous behavior of Al dimer signal.

Figure 4 Depth profile of ^{28}Si implant in Si wafer using negative secondary detection. Note enhanced Si dimer signal in region just below the surface as well as peaking of all signals at 450 seconds.

Figure 5 Depth profile of ^{28}Si implant in Si, this time monitoring positive secondaries. Implant peak is no longer visible, however all species show enhancement in the immediate sub-surface region.

Figure 6 Energy spectra of various secondary ions formed by O_2^+ bombardment of Dy_2O_3 (signal is plotted on a log scale in this and all following energy spectra).

Figure 7 Energy spectra of ions observed during O_2^+ bombardment of Gd_2O_3.

Figure 8 Energy spectra of ions from the same sample as Figure 7. In this case however, an Ar^+ primary beam was used; only the O^+ secondary ion shows behavior different from that observed in Figure 7.

Figure 9 Energy spectra of ions observed with O_2^+ bombardment of Gd foil.

Figure 10 Energy spectra of ions observed during O_2^+ bombardment of Tm_2O_3. The Tm^+ and TmO^+ spectra are shown as collected with and without a signal restricting aperature.

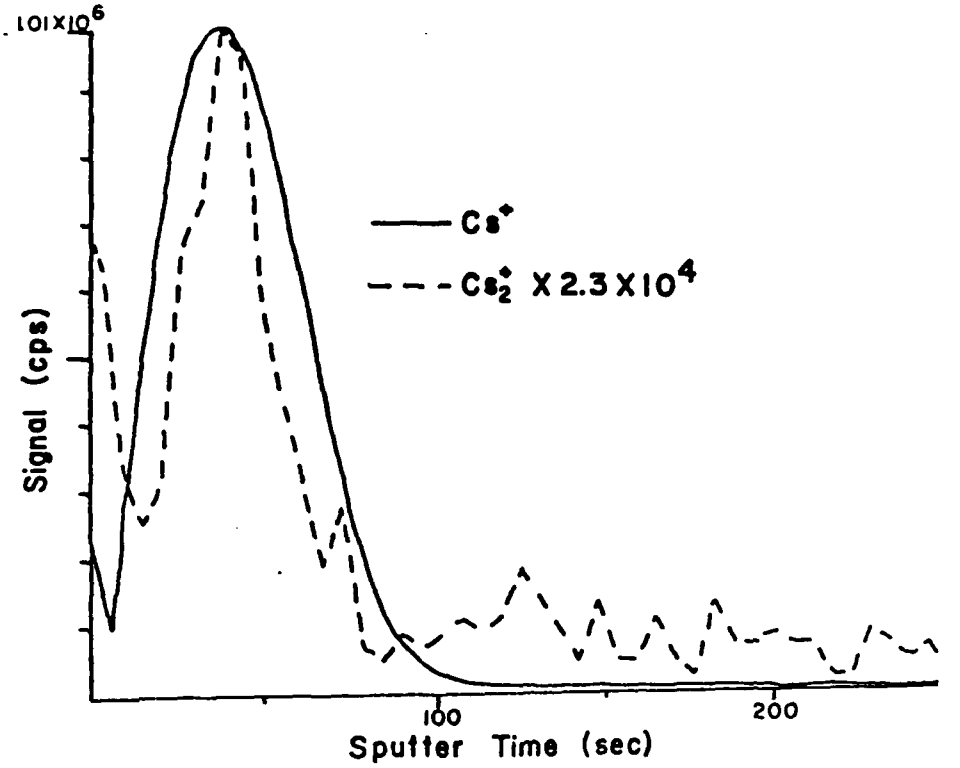
1.01X10^6
Cs+
Cs2+ X2.3X10^4
Signal (cps)
100
200
Sputter Time (sec)

Fig. 1

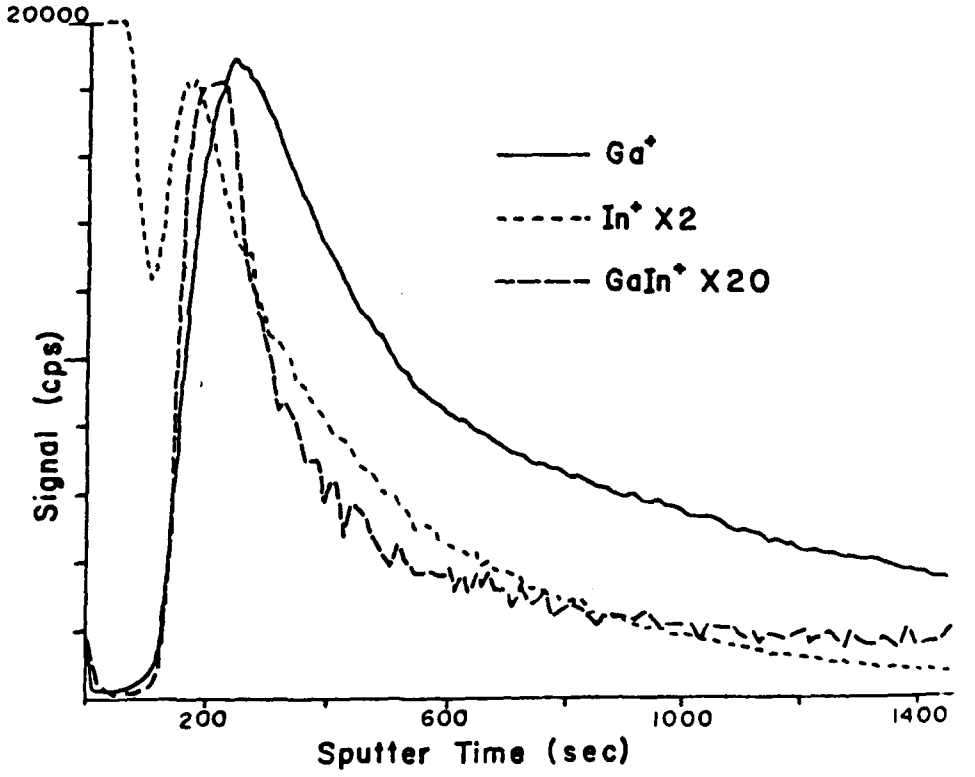
20000
Ga+
In+ X2
GaIn+ X20
Signal (cps)
200
600
1000
1400
Sputter Time (sec)

Fig. 2

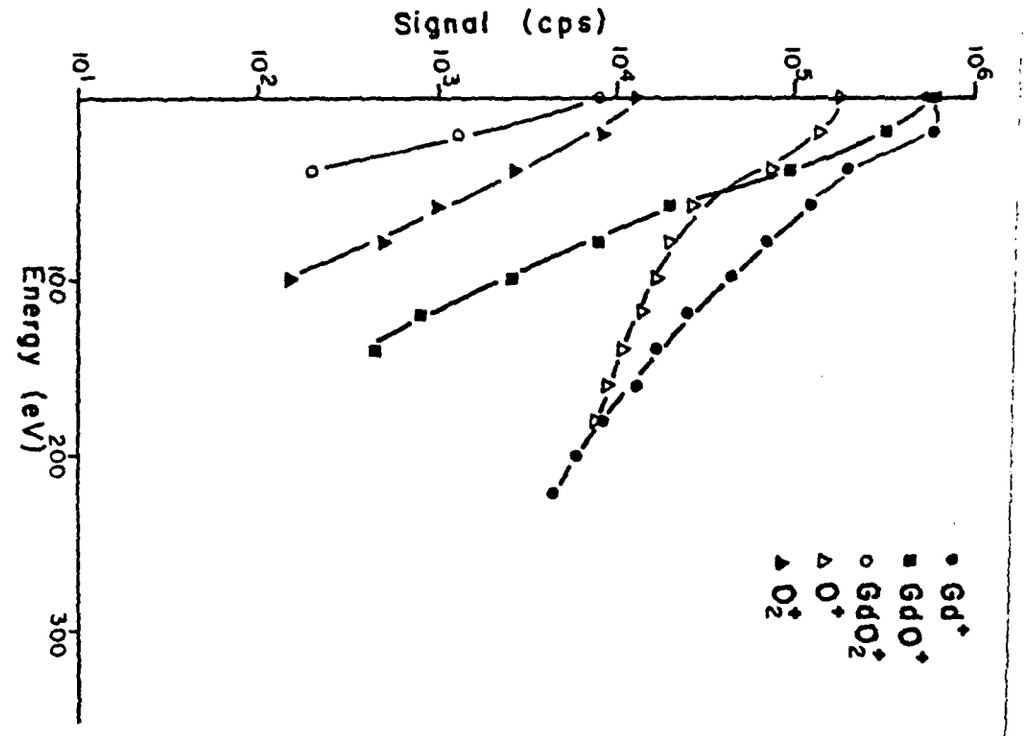

Fig. 7

Fig. 7

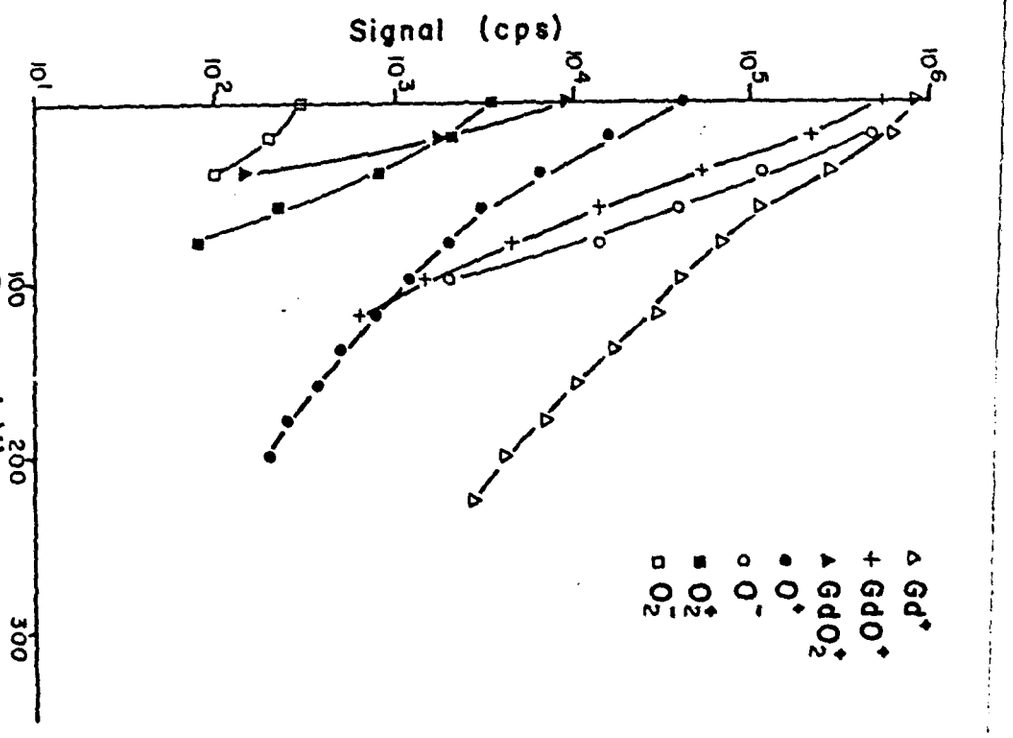

Fig. 8

Fig. 8

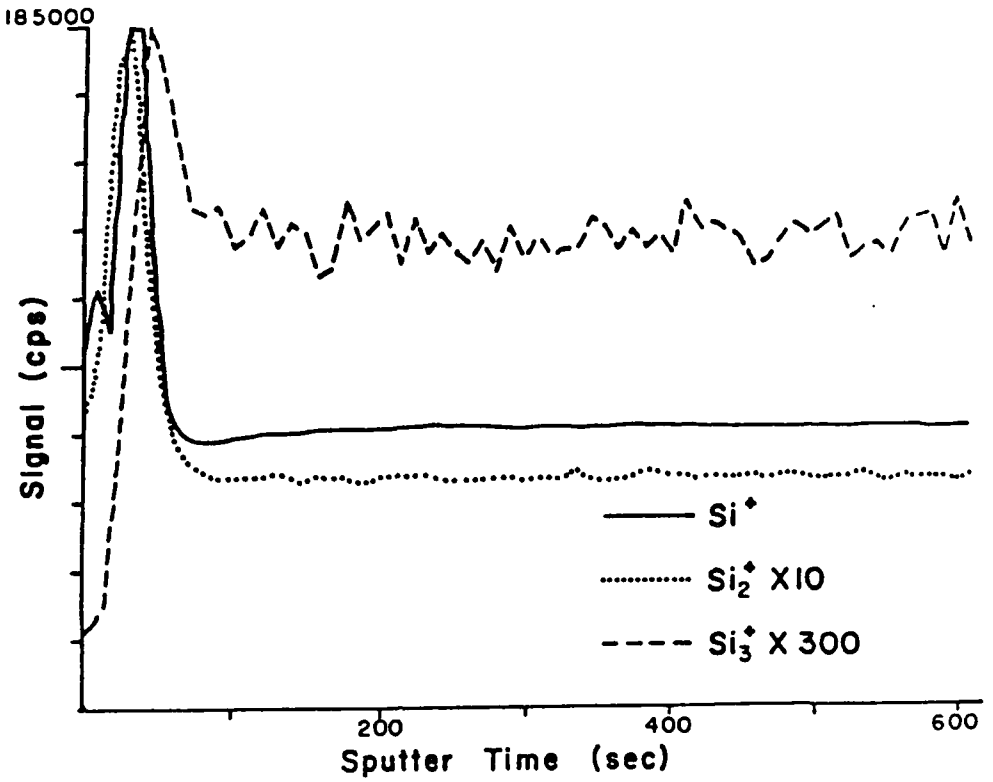
185000
Signal (cps)
Si+
Si2+ X10
Si3+ X 300
200
400
600
Sputter Time (sec)

Fig. 5

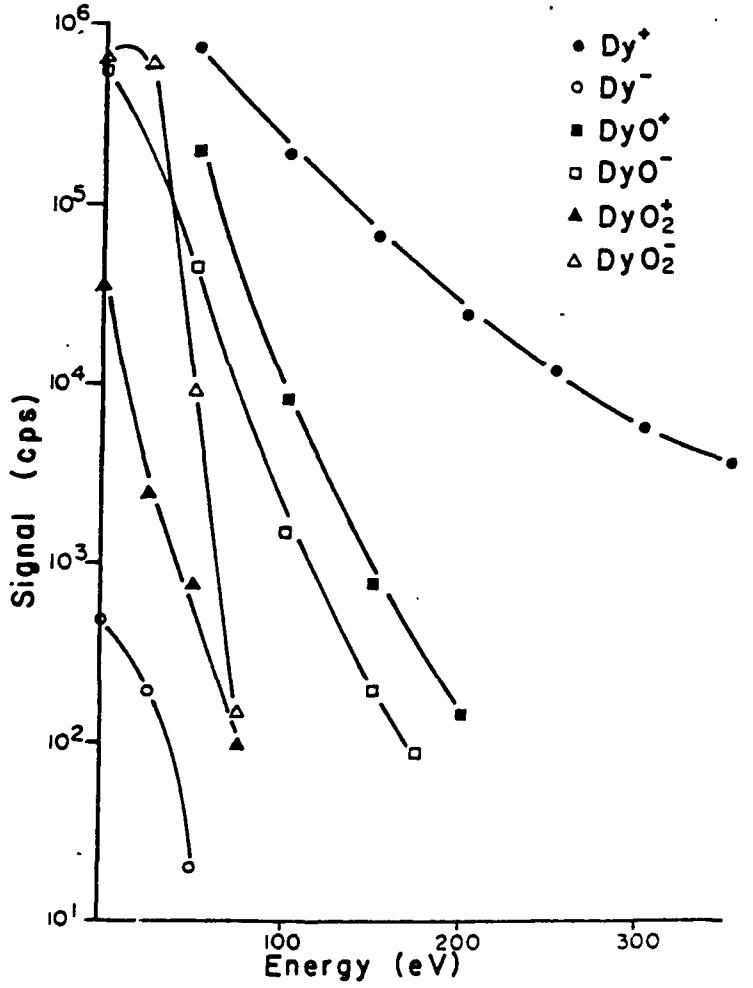
Dy+
Dy−
DyO+
DyO−
DyO2+
DyO2−
Signal (cps)
Energy (eV)

Fig. 6

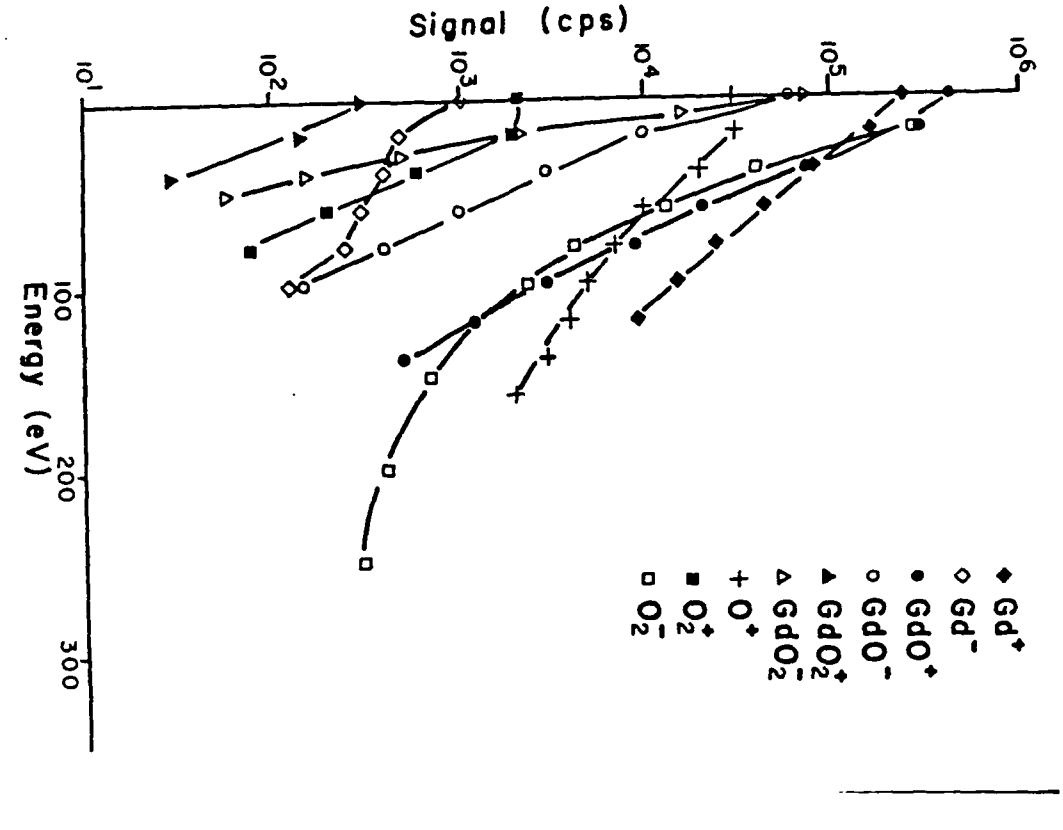

Fig. 9

Fig. 9

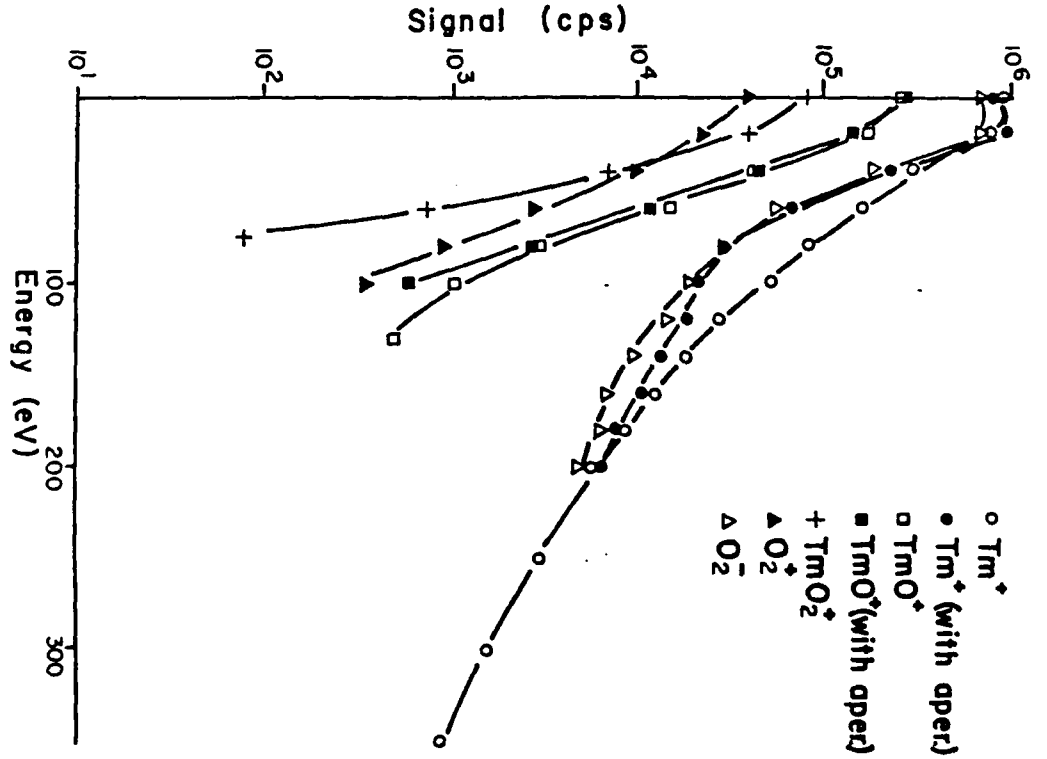

Fig. 10

Fig. 10

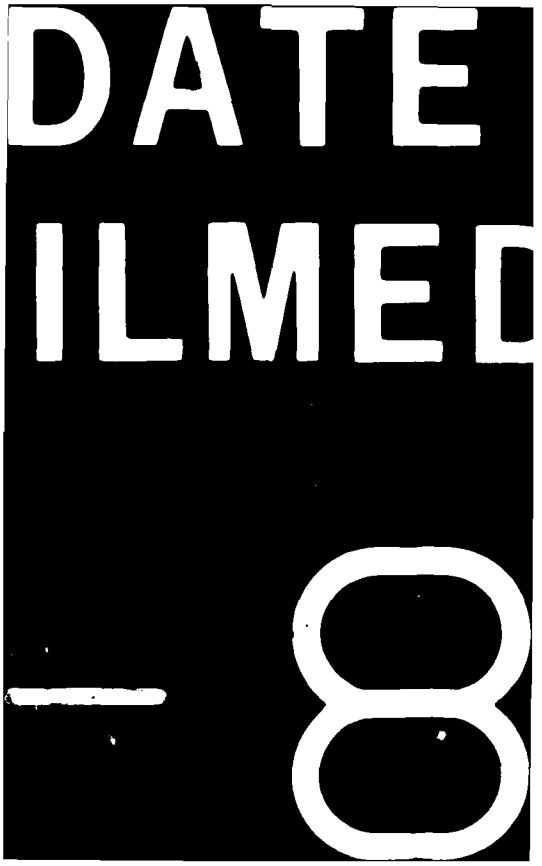
DATE
ILMED
8